Atmospheric
Measurement
Techniques

Note on rotational-Raman scattering in the O$_2$ A- and B-bands

A. Vasilkov[1]**, J. Joiner**[2]**, and R. Spurr**[3]

[1]Science Systems and Applications Inc., Lanham, MD, USA
[2]NASA Goddard Space Flight Center, Greenbelt, MD, USA
[3]RT Solutions Inc., Cambridge, MA, USA

Correspondence to: A. Vasilkov (alexander.vasilkov@ssaihq.com)

Abstract. Quantifying the impact of rotational-Raman scattering (RRS) on the O$_2$ A- and B-bands is important as these bands can be used for cloud and aerosol characterization for trace-gas retrievals including CO$_2$ and CH$_4$. In this paper, we simulate the spectral effects of RRS for various viewing geometries and instruments with different spectral resolutions. We also examine how aerosols affect the amount of RRS filling-in. We show that the filling-in effects of RRS are relatively small, but not negligible, in these O$_2$ absorption bands, particularly for high-spectral-resolution instruments. For comparison, we also compare and contrast the spectral signatures of RRS with those of terrestrial chlorophyll fluorescence.

1 Introduction

Near-InfraRed (NIR) retrievals of trace-gas concentrations, such as of CO$_2$ and CH$_4$, as well as terrestrial chlorophyll fluorescence often use information derived from O$_2$ A and B absorption band measurements (e.g., Reuter et al., 2010; Yoshida et al., 2011; Crisp et al., 2012; Guanter et al., 2010; O'Dell et al., 2012). Additive signals that contribute to satellite-measured top-of-the-atmosphere (TOA) radiance in the O$_2$ A- and B-bands can bias these retrievals. One type of additive signal that can produce a filling-in of deep telluric NIR absorption features, such as those in the O$_2$ A- and B-bands, is atmospheric rotational-Raman scattering (RRS) of N$_2$ and O$_2$ molecules. RRS has been neglected in the NIR spectral region, because the amount of atmospheric molecular scattering is low at these wavelengths. RRS effects in the O$_2$ A-band have been quantified in the literature (Sioris and Evans, 2000). RRS filling-in effects have also

been compared with those of fluorescence for several solar Fraunhofer lines in the visible and near infrared (Sioris et al., 2003). However, RRS effects are worthy of further consideration, owing to the high accuracy and precision requirements placed on CO$_2$ retrievals to be used for carbon assessment (e.g., Crisp et al., 2004).

Recent advances in the satellite retrieval of chlorophyll fluorescence in the NIR (Guanter et al., 2007, 2010, 2012; Joiner et al., 2011, 2012; Frankenberg et al., 2011a,b) also call into question the role of RRS in this spectral region. For example, Joiner et al. (2011, 2012) examined the filling-in of various solar Fraunhofer lines in the NIR and found the effects to be generally small, but not negligible. Frankenberg et al. (2012) showed that systematic biases in xCO$_2$ can be as large as 1 ppm if chlorophyll fluorescence in the O$_2$ A-band, amounting to 1 % to the continuum level radiance, is neglected. While RRS was not considered in that paper, it produces similar spectral effects on TOA radiances and should be examined in that context.

In this paper, we detail the effects of RRS in the O$_2$ A- and B-bands under various conditions. For comparison, we simulate the effects of chlorophyll fluorescence in the same bands. We also examine the impact of aerosol and thin clouds on both RRS and fluorescence additive signals within these absorption bands.

2 Radiative transfer simulations

2.1 Rotational-Raman scattering

We compute inelastic rotational-Raman scattering (RRS) in the O$_2$ A- and B-bands using the LInearized Discrete Ordinate Radiative Transfer (LIDORT-RRS) code (Spurr et al.,
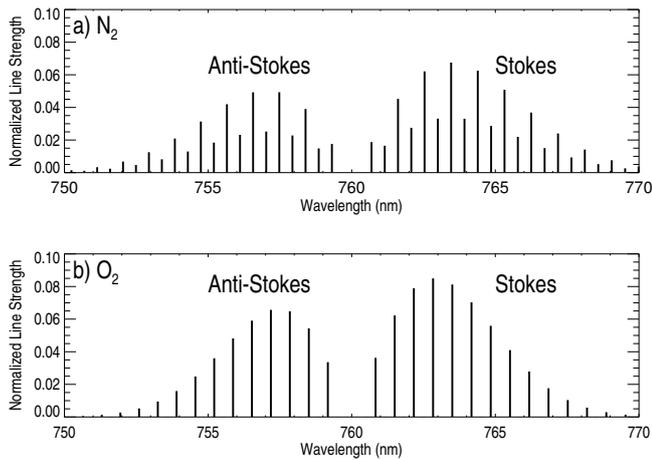
Fig. 1. Rotational-Raman spectra of **(a)** N_2 and **(b)** O_2 for excitation wavelength 760 nm. Line strengths are normalized such that the sum over all lines is equal to unity.

2008). LIDORT-RRS allows for accurate radiative transfer (RT) calculations in the presence of cloud/aerosol scattering. Oxygen absorption coefficients are calculated using a line-by-line code with spectroscopic absorption line parameters from the HIgh-resolution TRANsmission (HITRAN) molecular absorption database (Rothman et al., 2005) and the Voigt line shape profile. A single mid-latitude profile of temperature/pressure was used in the computation of the absorption coefficients.

For reference, Fig. 1 shows the rotational-Raman spectra of N_2 and O_2 computed as in Joiner et al. (1995) at a temperature of 273 K for an excitation wavelength near the O_2 A-band (760 nm). The rotational-Raman lines peak at around ± 3–4 nm from the excitation wavelength and extend to approximately ± 10 nm. Therefore, the spectral response of RRS is not the same as that for an additive signal as is more the case for chlorophyll fluorescence. However, the overall spectral effects of the RRS and fluorescence signals are similar, as will be shown below.

2.2 Chlorophyll fluorescence

The TOA fluorescence signal is calculated approximately using the quasi-single scattering approximation, i.e.,

$$I_f(\lambda) = I_{f0}(\lambda) \exp[-(\tau_a(\lambda) + \tau_s + \tau_R(\lambda)/2)/\cos(\theta)], \qquad (1)$$

where I_{f0} is the fluorescence radiance at the surface (assumed to be isotropic), θ is the viewing zenith angle (VZA), $\tau_a(\lambda)$ and $\tau_R(\lambda)$ are the absorption and Rayleigh optical thicknesses of the atmosphere, respectively, and $\tau_s = \tau(1 - g)$ is the scaled aerosol optical thickness, where τ is the aerosol optical thickness (assumed to be spectrally independent within the O_2 A-band) and g is the asymmetry parameter of the aerosol phase function. For non-absorbing wave-

lengths, this approach is applicable for low values of the scaled scattering optical thickness.

The far-red fluorescence radiance feature at the canopy level is approximated by a Gaussian function similar to Subhash and Mohanan (1997) and Zarco-Tejada et al. (2000); i.e., $I_{f0}(\lambda) = I_{fp} \exp[-(\lambda - \lambda_0)^2/(2\sigma^2)]$, where $\lambda_0 = 736.8$ nm and $\sigma = 21.2$ nm for the O_2 A-band and $\lambda_0 = 685.2$ nm and $\sigma = 9.6$ nm for the O_2 B-band. We assume a peak fluorescence value $I_{fp} = 2$ mW m^2 sr^{-1} nm^{-1} at a solar zenith angle (SZA) of 45° for both bands. This gives a surface fluorescence radiance at 762 nm of ~ 1.0 mW m^2 sr^{-1} nm^{-1}. This value of surface fluorescence radiance near the O_2 A-band is typical of observed terrestrial chlorophyll fluorescence values within the O_2 A-band spectral range and corresponds to approximately 1 % of the continuum level radiance at a surface albedo of 30 %.

2.3 Satellite instrument simulation

Quasi-monochromatic computations are carried out at a spectral sampling of 0.01 nm, that of the solar irradiance reference spectrum from Chance and Kurucz (2010) in which high-spectral-resolution spectra were convolved with a Gaussian response function with a full width at half maximum (FWHM) of 0.04 nm. For evaluation purposes, we also perform a limited number of RT computations with higher spectral resolution and sampling (sampled at 0.001 nm) using the solar irradiance spectrum from kurucz.harvard.edu/sun/irradiance2005/irradthu.dat in Appendix C. The latter sampling requires an order of magnitude more computational resources for a given calculation.

Computed TOA radiances are convolved with Gaussian response functions having various values of the FWHM. The chosen FWHMs (0.03, 0.1, 0.5, and 1 nm) are representative of existing and future satellite instruments. They include high-spectral-resolution instruments such as the Fourier Transform Spectrometer (FTS) on the Japanese Greenhouse gases Observing SATellite (GOSAT) (Kuze et al., 2009) and the Orbiting Carbon Observatory 2 (OCO-2) (Crisp et al., 2004) and moderate-spectral-resolution instruments such as the SCanning Imaging Absorption spectroMeter for Atmospheric CHartographY (SCIAMACHY) instrument aboard EnviSat (Gottwald et al., 2006) and the proposed FLourescence EXplorer (FLEX) (Rascher, 2007). However, note that convolution of these instrument response functions with the solar spectrum of Chance and Kurucz (2010) (that has spectral resolution similar to our highest spectral resolution simulation) will somewhat underestimate solar line filling as shown in Appendix C.

For reference, the solar irradiance spectrum convolved with the chosen response functions is shown in Fig. 2 in the spectral ranges selected around the O_2 A- and B-bands. It is seen that these spectral ranges contain several deep Fraunhofer lines. RRS fills in Fraunhofer lines due to spectral
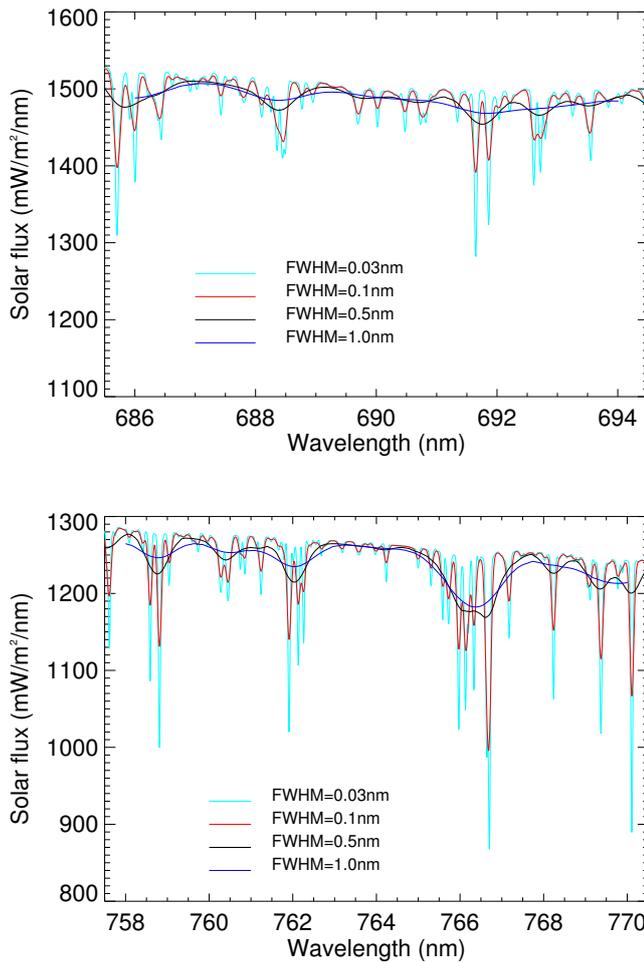
Fig. 2. Solar irradiance in the vicinity of O_2 B (top) and O_2 A (bottom) bands.

Fig. 3. TOA radiances, inelastic (top) and elastic (bottom) for SZA = 45°, at nadir, and surface reflectivity 0.3.

transport of energy from wavelengths in the vicinity of the lines. The filling-in is larger for deeper lines.

2.4 Surface specification and viewing geometries

For simplicity, we assumed a spectrally independent Lambertian surface with reflectivities $R = 30\%$ in the O_2 A-band and 5% in the O_2 B-band. These values are typical for vegetated surfaces. The TOA simulations are performed for three solar zenith angles (20, 45, and 70°) at various viewing zenith and azimuth angles appropriate for typical satellite observations.

3 Results and discussion

3.1 RRS effects for molecular scattering only

Figure 3 shows TOA elastic (I_e) and inelastic (I_{rrs}) RRS radiances calculated for SZA = 45° and observations at nadir for a clean sky (i.e., aerosol free). The inelastic RRS radi-

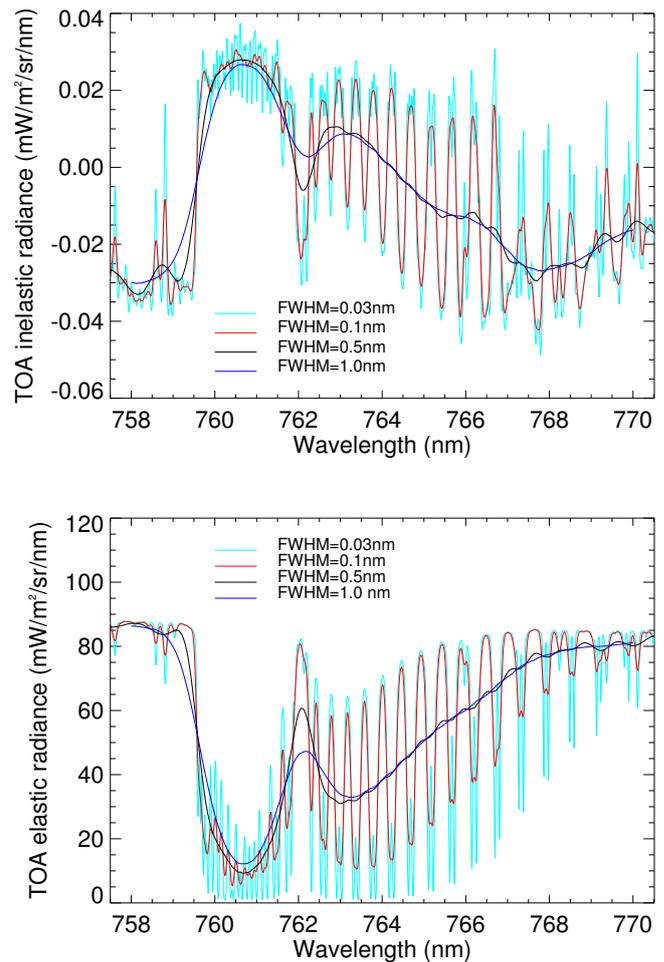ances are small as compared with the elastic radiances, I_e. The inelastic radiances are positive within the O_2 A-band where the amount of outgoing Raman scattered light from those wavelengths is less than the amount of incoming Raman scattered light from excitation wavelengths in the surrounding continuum. The reverse is true of wavelengths near to or in the shoulders surrounding the O_2 A-band.

Figure 4 shows the percent difference between the total and elastic radiances, also known as the filling-in factor, i.e., $I_{rrs}/I_e \times 100$ (in %) (Joiner et al., 1995) for wavelengths in and surrounding the O_2 A- and B-bands. Within deep telluric O_2 A-band absorption lines where elastic radiances are small, the filling-in can be as large as 2% for high-spectral-resolution instruments. Note that the filling-in does not decrease linearly with increasing FWHM within the O_2 A-band. For relatively low-resolution instruments (FWHM = 1 nm), the maximum filling-in within the O_2 A-band is < 0.2%.

It can be seen that values of the RRS filling-in in the O_2 B-band are significantly lower than in the O_2 A-band despite

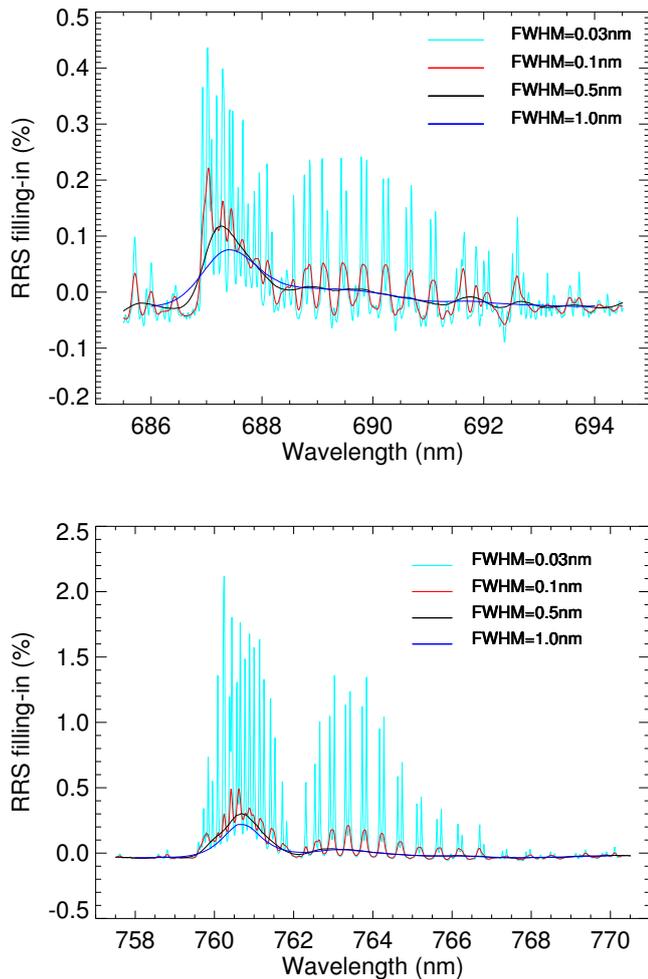**Fig. 4.** Percentage of filling-in from RRS for SZA = 45°, at nadir, for wavelengths in and around the O$_2$ B-band and surface reflectivity 0.05 (top) and O$_2$ A-band and surface reflectivity 0.3 (bottom).

the fact that there is more atmospheric scattering at the O$_2$ B-band. This is explained by the fact that absorption lines in the O$_2$ A-band are much deeper than in the O$_2$ B-band. Thus, the filling-in from Raman scattered light coming from excitation wavelengths in the surrounding continuum in terms of percent of radiance is larger in the O$_2$ A-band than in the O$_2$ B-band. The remainder of the paper will therefore focus primarily on the filling-in of the O$_2$ A-band.

3.2 RRS viewing angle dependences

The VZA dependence of the maximum RRS filling-in at wavelengths with large RRS effects within the O$_2$ A-band (760–762 nm) is shown in Fig. 5 for SZA = 45 and 70° at azimuth angle of 90°. The RRS filling-in increases with VZA, owing to increased photon path lengths and thus increased probability of Raman scattering. At SZA = 45°, the filling-in at 60° VZA doubles as compared with that at nadir.
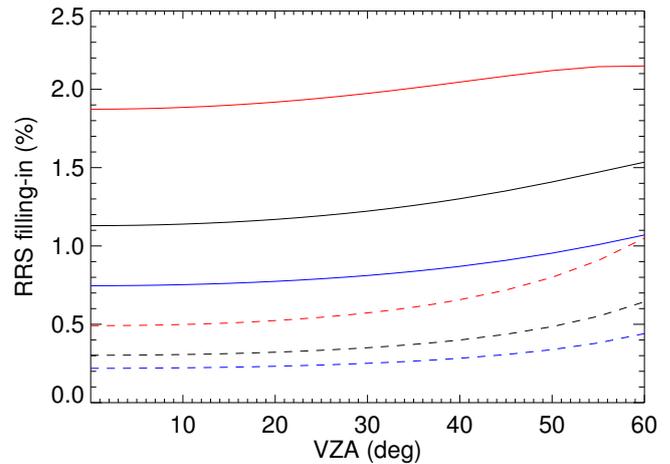

Fig. 5. Maximum percentage of filling-in due to RRS within 760–762 nm, as a function of VZA for SZA = 45° (dashed line) and 70° (solid line) and relative azimuth angle of 90°. Red: FWHM 0.1 nm. Black: FWHM 0.5 nm. Blue: FWHM = 1.0 nm.

3.3 Comparison of RRS and fluorescence spectral signatures

Figure 6 shows the TOA fractional fluorescence radiance (defined as a ratio of fluorescence radiance to elastic radiance) computed for SZA = 45° and observations at nadir at wavelengths in and surrounding the O$_2$ A- and B-bands. For this viewing geometry and a substantial amount of assumed chlorophyll fluorescence (2 mW m^{-2} sr^{-1} nm^{-1} at the two emission peaks), the fractional fluorescence signal is significantly higher than that of RRS. The spectral effects of fluorescence and RRS filling-in are similar within this spectral region though some small differences are observed. For example, the fluorescence spectral response contains a slight tilt across this wavelength range, owing to the Gaussian shapes of the emission features.

The relative ratio of fluorescence to RRS filling-in within the O$_2$ A-band depends upon the FWHM. At high spectral resolution (FWHM = 0.03 nm), the fractional fluorescence signal exceeds that of RRS by a factor of about 2 at the center of the O$_2$ A-band, while at FWHM = 1.0 nm fluorescence is larger than RRS by a factor of 6.4. Note that we have subtracted the fluorescence signal in the continuum from the total fluorescence signal to enhance the spectral comparison with RRS effects.

The O$_2$ B-band is spectrally located near the peak of the 685 nm fluorescence emission feature. Therefore, the total percentage of the contribution of fluorescence to the TOA radiance is much higher in the O$_2$ B-band as compared with the O$_2$ A-band. However, when the fluorescence signal is normalized with respect to the continuum, the relative fluorescence contribution to the TOA radiance in the O$_2$ B-band is somewhat lower than in the O$_2$ A-band. This is explained by
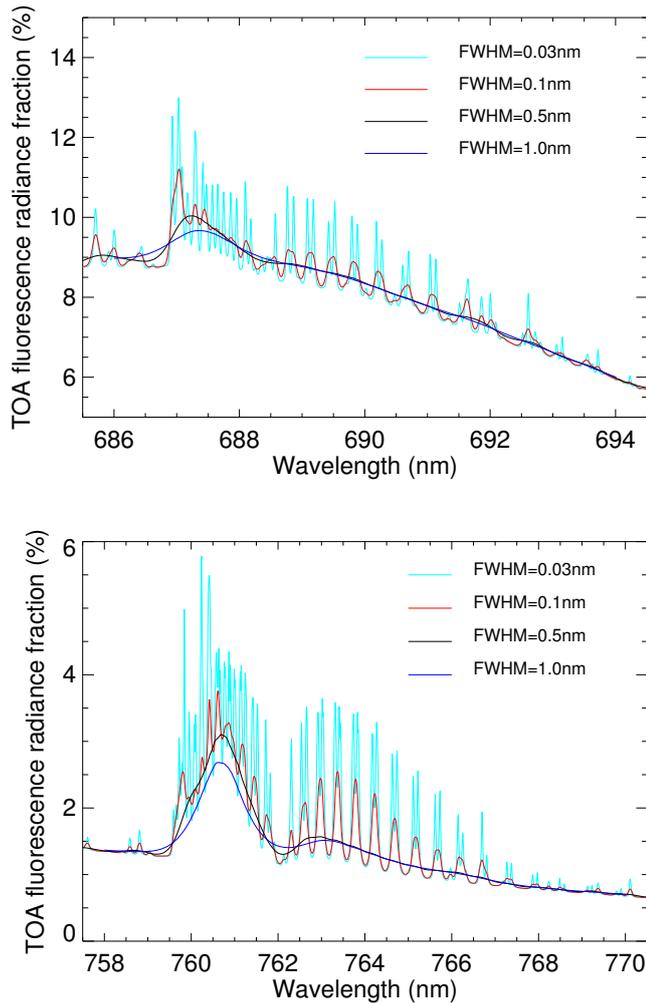
Fig. 6. Percentage of the contribution of fluorescence emission to TOA radiance for SZA = 45°, at nadir, for wavelengths in and surrounding the O_2 B-band and surface reflectivity 0.05 (top) and O_2 A-band and surface reflectivity 0.3 (bottom).

Fig. 7. Comparison of fractional radiance effect of RRS (red), fluorescence (blue), and surface pressure change (ΔP_s) of 3 hPa (green) for FWHM = 0.1 nm, SZA = 45°, at nadir, for wavelengths in and surrounding the O_2 B-band and surface reflectivity 0.05 (top) and O_2 A-band and surface reflectivity 0.3 (bottom). All curves normalized to a value of zero at 686 nm (top) and 758 nm (bottom).

deeper absorption lines in the O_2 A-band as compared with the O_2 B-band.

A direct comparison of the spectral RRS and fluorescence signals at wavelengths in and surrounding the O_2 A- and B-bands is shown in Fig. 7 for FWHM = 0.1 nm along with the radiance response for a surface pressure change of 3 hPa. Again for clarity, the fluorescence spectral response has been normalized with respect to the continuum value. A value of 0.5 mW m^{-2} sr^{-1} nm^{-1} is used for the peak fluorescence. At this low level of fluorescence radiance, the fractional RRS and fluorescence signals are similar, and both are also similar in magnitude to the small surface pressure change. However, there are some subtle differences. For example, surface pressure change does not fill in solar Fraunhofer lines, whereas both RRS and fluorescence produce a solar filling-in signal. It should be noted that the spectral RRS, fluorescence, and response for a surface pressure change in the O_2 B-band are
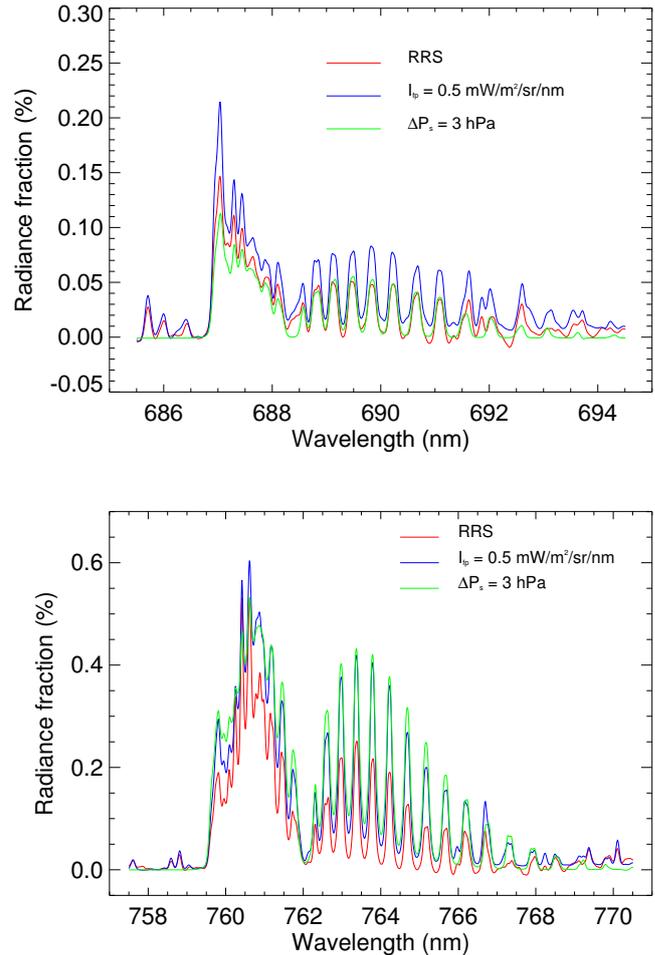
lower than in the O_2 A-band by a factor of approximately 3 due to less-deep absorption lines in the O_2 B-band.

3.4 Aerosol and cloud effects on RRS

We carried out RT computations in the presence of aerosol/cloud with various optical depths and layer heights. Aerosol/cloud scattering is assumed to be in accordance with the Henyey–Greenstein (H–G) phase function with an asymmetry factor of 0.7 for aerosol and 0.85 for clouds. The simplified H–G phase function is adequate for our purpose of examining the qualitative effects of aerosol/cloud on RRS and fluorescence. We characterize the aerosol scattering effect on RRS (fluorescence) through a fractional difference of the TOA inelastic (fluorescence) radiance between aerosol and aerosol-free cases: $(I_r(\tau) - I_r(\tau = 0))/I_e(\tau = 0) \times 100$ (in %), where I_r is either RRS I_{rrs} or fluorescence I_f radiance and
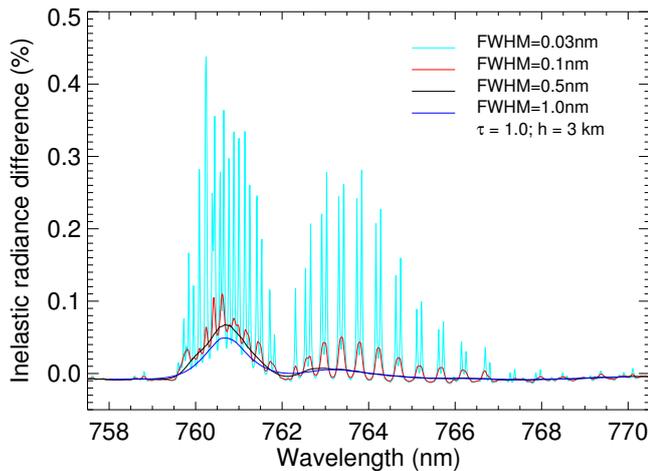
Fig. 8. Fractional inelastic radiance difference between aerosol loading with $\tau = 1.0$ and aerosol-free case, SZA $= 45°$, at nadir, and surface reflectivity 0.3.

τ is the aerosol optical depth. Figure 8 shows the fractional difference of the TOA inelastic radiance for a nonabsorbing aerosol plume with $\tau = 1.0$. The aerosol plume has a geometrical thickness of 1 km with a plume-top height of 3 km. In general, the aerosol effect on RRS is small. The presence of aerosol increases inelastic radiance within oxygen absorption lines and decreases it beyond the absorption lines, i.e., in the continuum. The total aerosol effect is complex because of two opposing tendencies. Aerosol partly screens the atmosphere below the plume, decreasing photon path lengths. However, aerosol also increases photon path length, owing to scattering between the bright ground and aerosol layer. The relative increase of the inelastic radiance owing to aerosol is larger for lower values of the FWHM. The aerosol effect on inelastic radiance depends on aerosol optical depth and height. RT computations for $\tau = 0.15$ show that the effect decreases by a factor of ~ 4 as compared with $\tau = 1.0$. Increase of the aerosol plume height also decreases the aerosol effect on RRS. For example, the aerosol effect at $\tau = 1.0$ decreases by a factor of ~ 1.8 when the aerosol height increases from 3 to 10 km.

We looked at the cloud effect on RRS in terms of the maximum of the fractional inelastic radiance difference between cloudy and cloud-free cases. The presence of low-altitude clouds substantially increases the cloud effect on RRS with increasing cloud optical depth (COD). Varying COD from 1 to 50 enhances the cloud effect on RRS by a factor of approximately 2. For brighter clouds, i.e., optically thicker clouds, the increase of photon paths above the cloud due to reflection from the cloud prevails over the decrease of RRS due to screening of the atmosphere below the cloud. The presence of high-altitude clouds mostly decreases the cloud effect on RRS with increasing COD; i.e., screening of the atmosphere below the cloud plays the main role. However, optically thin
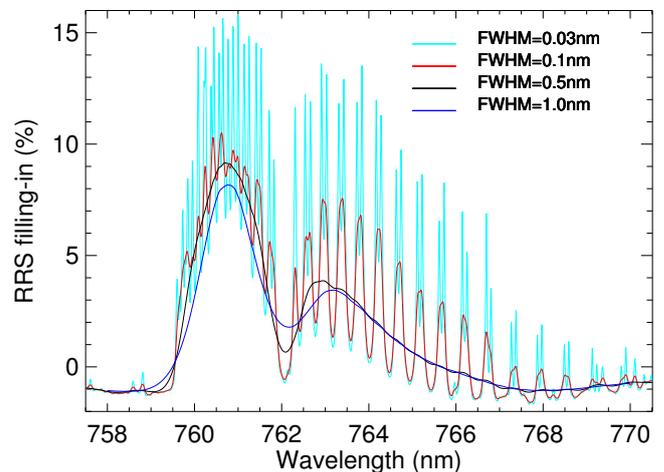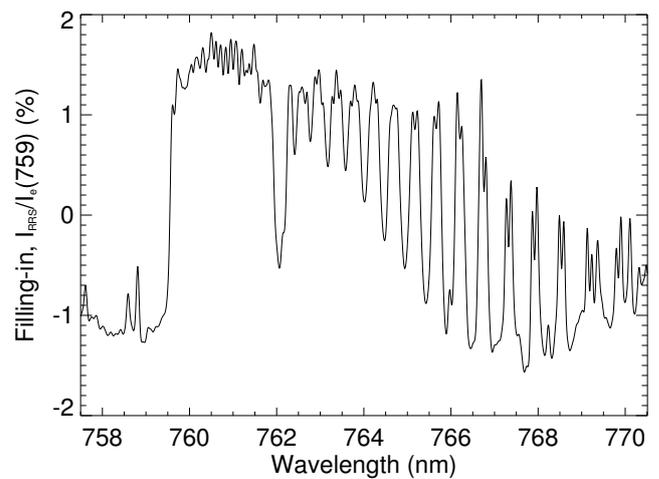

Fig. 9. Top: RRS filling-in computed for conditions similar to Sioris and Evans (2000) with their definition of filling-in (see text). Bottom: filling-in computed for the same conditions with our definition and different spectral resolutions.

clouds can slightly increase the cloud effect on RRS as compared with cloud-free case. This case is quite similar to the aerosol effect discussed in the previous paragraph.

The aerosol effect on the TOA fluorescence is quite simple: the presence of aerosol reduces the fluorescence signal according to Eq. (1). The fractional TOA fluorescence radiance difference between aerosol and aerosol-free cases, i.e., the difference normalized by the TOA radiance, significantly depends on wavelength. It is interesting that the presence of aerosol reduces the fractional fluorescence signal most substantially in the spectral range of strong absorption.

4   Conclusions

RRS produces a signal within the O_2 A- and B-bands spectrally similar to that produced by chlorophyll fluorescence
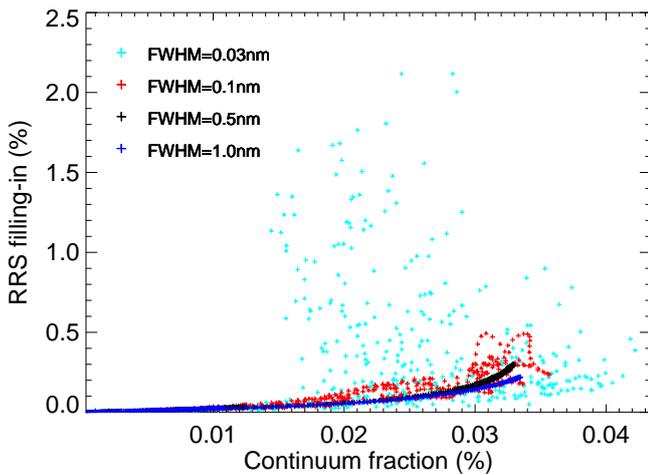
Fig. 10. RRS signal defined as a percentage of the spectral elastic radiance versus the RRS signal defined as a percentage of the continuum level radiance at 758 nm. Every point represents a wavelength around the O_2 A-band. Only positive filling-in values are shown. Input parameters are similar to those used in Fig. 4.
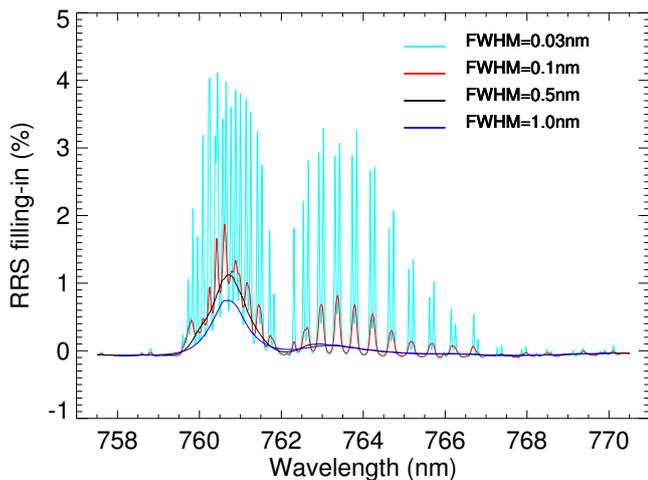

Fig. 12. Similar to Fig. 4 but computed with the higher-spectral-sampling solar irradiance (0.001 nm).

Fig. 11. Similar to Fig. 4 but SZA = 70°.

Fig. 13. Maximum percentage of filling-in within 760–762 nm due to RRS as a function of surface albedo for SZA = 45° at nadir.

and variations in surface pressure. At moderate solar zenith angles, the magnitude of RRS filling-in is similar to that from a terrestrial chlorophyll fluorescence emission with the peak value of $\sim 0.5\,\mathrm{mW\,m^{-2}\,sr^{-1}\,nm^{-1}}$ or from a surface pressure change of $\sim 3\,\mathrm{hPa}$. The RRS filling-in of O_2 absorption lines increases for larger SZAs and VZAs. The percentage of RRS filling-in in the O_2 B-band is less than in the O_2 A-band. The presence of a low-altitude aerosol plume may slightly increase inelastic radiance and thus increase RRS filling-in. For an aerosol plume with $\tau = 1$ and height of 3 km, the fractional RRS filling-in increases by about 30 % in the center of the O_2 A-band as compared with the aerosol-free atmosphere.

Note that our definition of RRS filling-in differs from that of Sioris and Evans (2000), who define it as a percentage
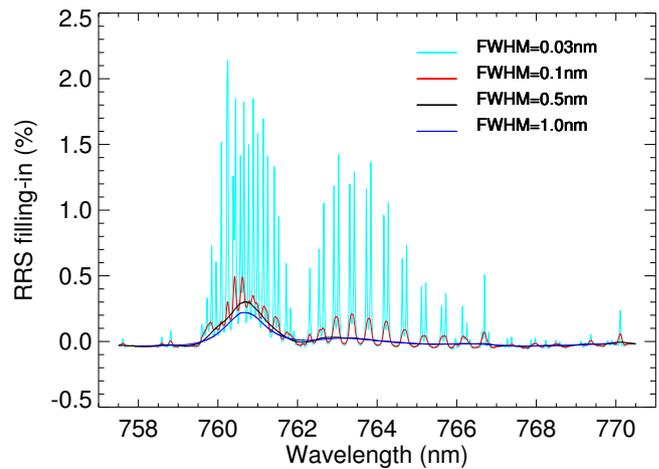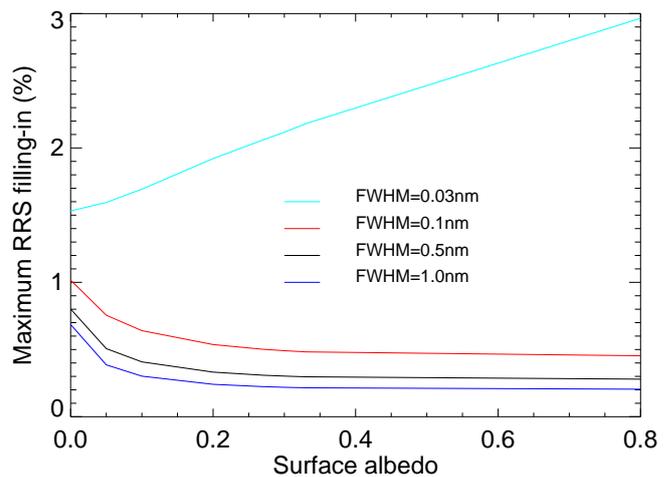
of the continuum radiance. We provide an example of direct comparison of both definitions in Appendix A. Use of different definitions of filling-in may lead to somewhat different conclusions regarding the importance of RRS, particularly within the O_2 A-band. Our calculations and definition lead to the conclusion that while the RRS effect is small it may be non-negligible even at moderate solar zenith angles with respect to fluorescence and surface pressure retrievals relevant also to $x\mathrm{CO_2}$ retrievals. However, this conclusion may depend upon the level of instrumental noise for a given instrument, particularly for high-spectral-resolution instruments that resolve deep absorption lines. For such instruments, high values of the RRS filling-in, defined as the ratio of inelastic radiance to elastic radiance, may be close to the noise level within the cores of deep absorption lines that produce low radiances.

It has been shown that a fluorescence signal of 1 % of the continuum level radiance around the O_2 A-band may bias xCO_2 retrievals by $\sim$1 ppm (Frankenberg et al., 2012). Assuming linearity under similar conditions, RRS may produce a bias of the order of 0.25 ppm in xCO_2. Note that comparable TOA RRS and fluorescence filling-in signals using our filling-in definition result from different originating radiance values when defined in terms of continuum level radiances (typical RRS radiances are $\sim$ 0.04 % of the continuum level radiance in the O_2 A-band at surface albedo of 0.3 for instruments with spectral resolution better than 0.1 nm). At first look, the comparable RRS and moderately low fluorescence spectral filling-in signals (with our definition) in the O_2 A-band may seem to be paradoxical, because RRS radiances are much lower than fluorescence radiances in terms of percentage of the continuum radiance. An explanation of this paradox lies in different mechanisms of formation of TOA RRS and fluorescence signals. Fluorescence, emitted at the surface, is strongly attenuated by oxygen absorption when passing to the top of the atmosphere. The RRS radiance is produced by Raman scattering throughout the entire atmospheric photon path. Even though the RRS photons produced in the lower layers of the atmosphere can be absorbed by layers above, the end effect is that significant TOA RRS filling-in can be produced with relatively low values of RRS radiance as compared with fluorescence.

Appendix A

Comparison of filling-in with results of Sioris and Evans (2000)

The focus of our work is somewhat different from that of Sioris and Evans (2000) who presented calculations primarily at high solar zenith angles (near 90°). Here, we attempt to reproduce the filling-in reported by Sioris and Evans (2000) for nadir observations at high SZA (89°) with surface albedo of zero. Our calculations are done with FWHM = 0.06 nm or $\sim 1 \, \text{cm}^{-1}$. Figure 9 shows the results where we define filling-in as in Sioris and Evans (2000), referencing the RRS radiance to that of the continuum. Our results are very comparable to those of Sioris and Evans (2000) in terms of both spectral dependence and magnitude. Figure 9 also shows computed filling-in as defined above and used throughout the manuscript. Our definition of filling-in provides much higher values within the O_2 A-band, particularly at high SZA. We directly compare two definitions of the RRS signal in Fig. 10 that shows RRS signal defined as a percentage of the spectral elastic radiance versus the RRS signal defined as a percentage of the continuum level radiance at 758 nm. Every wavelength is shown as a point on this plot.

Appendix B

Computed filling-in for SZA = 70°

For comparison, Fig. 11 is similar to Fig. 4 but shows the spectral RRS filling-in in the O_2 A-band for SZA = 70°. At high spectral resolution, the increase from SZA = 45° to SZA = 70° at the wavelength with the largest filling-in is about a factor of 2. At lower spectral resolution (FWHM = 1 nm) the increase is approximately a factor of 4.

Appendix C

Computed RRS filling-in with higher-spectral-resolution data

A comparison of the RRS filling-in computed using the reference solar irradiance from Chance and Kurucz (2010) and the solar irradiance with higher spectral sampling from kurucz. harvard.edu/sun/irradiance2005/irradthu.dat shows that differences between them are generally very small except for a few narrow and deep Fraunhofer lines beyond the O_2 A-band. The use of the higher-spectral-sampling solar irradiance produces larger values of the filling-in of those Fraunhofer lines (Fig. 12).

Appendix D

Computed RRS filling-in dependence on surface albedo

We carried out radiative transfer simulations in the O_2 A-band for values of the surface albedo between 0 and 0.8. Figure 13 shows that for moderate- and low-resolution instruments, the RRS filling-in dependence on surface albedo in the O_2 A-band is similar to that shown for filling-in of solar Fraunhofer lines (see Fig. 2 of Joiner et al. (2004), which also shows some variation in this behavior as a function of viewing geometry); at low surface albedos (between approximately 0 and 0.2), the filling-in decreases with increasing surface albedo. For high-resolution instruments, the telluric RRS filling-in increases with increasing surface albedo. The absorption line depth increases with increasing surface albedo. When individual absorption lines are spectrally resolved, the filling-in (defined as the ratio of inelastic radiance to the TOA radiance) then increases with surface albedo.

Figure 13 shows that the RRS filling-in dependence on surface albedo is very small in the albedo range of 0.2–0.8 (typical of vegetated and snow-covered land) for moderate- to low-resolution instruments. Variations for high-spectral-resolution instrument are larger and similar in magnitude to changes across a wide satellite swath as shown in Fig. 5. In addition, for low-resolution instruments the surface albedo dependence on RRS filling-in could be important for the O_2 B-band where surface albedos are typically lower over

land. We note that the surface albedo dependence may produce some spatial structure in the observed filling-in from space-based instruments.

Edited by: D. Loyola

References

Chance, K. and Kurucz, R. L.: An improved high-resolution solar reference spectrum for Earth's atmosphere measurements in the ultraviolet, visible, and near infrared, J. Quant. Spectrosc. Ra., 111, 1289–1295, 2010.

Crisp, D., Atlas, R. M., Breon, F.-M., Brown, L. R., Burrows, J. P., Ciais, P., Connor, B. J., Doney, S. C., Fung, I. Y., Jacob, D. J., Miller, C. E., O'Brien, D., Pawson, S., Randerson, J. T., Rayner, P., Salawitch, R. J., Sander, S. P., Sen, B., Stephens, G. L., Tans, P. P., Toon, G. C., Wennberg, P. O., Wofsy, S. C., Yung, Y. L., Kuang, Z., Chudasama, B., Sprague, G., Weiss, B., Pollock, R., Kenyon, D., and Schroll, S.: The Orbiting Carbon Observatory (OCO) mission, Adv. Space Res., 34, 700–709, 2004.

Crisp, D., Fisher, B. M., O'Dell, C., Frankenberg, C., Basilio, R., Bösch, H., Brown, L. R., Castano, R., Connor, B., Deutscher, N. M., Eldering, A., Griffith, D., Gunson, M., Kuze, A., Mandrake, L., McDuffie, J., Messerschmidt, J., Miller, C. E., Morino, I., Natraj, V., Notholt, J., O'Brien, D. M., Oyafuso, F., Polonsky, I., Robinson, J., Salawitch, R., Sherlock, V., Smyth, M., Suto, H., Taylor, T. E., Thompson, D. R., Wennberg, P. O., Wunch, D., and Yung, Y. L.: The ACOS CO_2 retrieval algorithm – Part II: Global XCO_2 data characterization, Atmos. Meas. Tech., 5, 687–707, doi:10.5194/amt-5-687-2012, 2012.

Frankenberg, C., Butz, A., and Toon, G. C.: Disentangling chlorophyll fluorescence from atmospheric scattering effects in O_2 A-band spectra of reflected sun-light, Geophys. Res. Lett., 38, L03801, doi:10.1029/2010GL045896, 2011a.

Frankenberg, C., Fisher, J. B., Worden, J., Badgley, G., Saatchi, S. S., Lee, J.-E., Toon, G. C., Butz, A., Jung, M., Kuze, A., and Yokota, T.: New global observations of the terrestrial carbon cycle from GOSAT: Patterns of plant fluorescence with gross primary productivity, Geophys. Res. Lett., 38, L17706, doi:10.1029/2011GL048738, 2011b.

Frankenberg, C., O'Dell, C., Guanter, L., and McDuffie, J.: Remote sensing of near-infrared chlorophyll fluorescence from space in scattering atmospheres: implications for its retrieval and interferences with atmospheric CO_2 retrievals, Atmos. Meas. Tech., 5, 2081–2094, doi:10.5194/amt-5-2081-2012, 2012.

Gottwald, M., Bovensmann, H., Lichtenberg, G., Noel, S., von Bargen, A., Slijkhuis, S., Piters, A., Hoogeveen, R., von Savigny, C., Buchwitz, M., Kokhanovsky, A., Richter, A., Rozanov, A., Holzer-Popp, T., Bramstedt, K., Lambert, J.-C., Skupin, J., Wittrock, F., Schrijver, H., and Burrows, J. P.: SCIAMACHY, Monitoring the Changing Earth's Atmosphere, Published by DLR and Springer, doi:10.1007/978-90-481-9896-2, 2006.

Guanter, L., Alonso, L., Gómez-Chova, L., Amorós-López, J., Vila-Francés, J., and Moreno, J.: Estimation of solar-induced vegetation fluorescence from space measurements, Geophys. Res. Lett., 34, L08401, doi:10.1029/2007GL029289, 2007.

Guanter, L., Alonso, L., Gómez-Chova, Meroni, M., Preusker, R., Fischer, J., and Moreno, J.: Developments for vegetation fluorescence retrieval from spaceborne high-resolution spectrometry in the O_2-A and O_2-B absorption bands, J. Geophys. Res., 115, D19303, doi:10.1029/2009JD013716, 2010.

Guanter, L., Frankenberg, C., Dudhia, A., Lewis, P. E., Gómez-Dans, J., Kuze, A., Suto, H., and Grainger, R. G.: Retrieval and global assessment of terrestrial chlorophyll fluorescence from GOSAT space measurements, Remote Sens. Environ., 121, 236–251, 2012.

Joiner J., Bhartia, P. K., Cebula, R. P., Hilsenrath, E., McPeters, R. D., and Park, H.: Rotational-Raman scattering (Ring effect) in satellite backscatter ultraviolet measurements, Appl. Opt., 34, 4513–4525, 1995.

Joiner, J., Vasilkov, A. P., Flittner, D. E., Gleason, J. F., and Bhartia, P. K.: Retrieval of cloud pressure and oceanic chlorophyll content using Raman scattering in GOME ultraviolet spectra, J. Geophys. Res., 109, D01109, doi:10.1029/2003JD003698, 2004.

Joiner, J., Yoshida, Y., Vasilkov, A. P., Yoshida, Y., Corp, L. A., and Middleton, E. M.: First observations of global and seasonal terrestrial chlorophyll fluorescence from space, Biogeosciences, 8, 637–651, doi:10.5194/bg-8-637-2011, 2011.

Joiner, J., Yoshida, Y., Vasilkov, A. P., Middleton, E. M., Campbell, P. K. E., Yoshida, Y., Kuze, A., and Corp, L. A.: Filling-in of near-infrared solar lines by terrestrial fluorescence and other geophysical effects: simulations and space-based observations from SCIAMACHY and GOSAT, Atmos. Meas. Tech., 5, 809–829, doi:10.5194/amt-5-809-2012, 2012.

Kuze, A., Suto, H., Nakajima, M., and Hamazaki, T.: Thermal and near infrared sensor for carbon observation Fourier-transform spectrometer on the Greenhouse Gases Observing Satellite for greenhouse gases monitoring, Appl. Opt., 48, 6716–6733, 2009.

O'Dell, C. W., Connor, B., Bösch, H., O'Brien, D., Frankenberg, C., Castano, R., Christi, M., Eldering, D., Fisher, B., Gunson, M., McDuffie, J., Miller, C. E., Natraj, V., Oyafuso, F., Polonsky, I., Smyth, M., Taylor, T., Toon, G. C., Wennberg, P. O., and Wunch, D.: The ACOS CO_2 retrieval algorithm – Part 1: Description and validation against synthetic observations, Atmos. Meas. Tech., 5, 99–121, doi:10.5194/amt-5-99-2012, 2012.

Rascher, U.: FLEX – Fluorescence EXplorer: A remote sensing approach to quantify spatio-temporal variations of photosynthetic efficiency from space, Photosynth. Res., 91, 293–294, 2007.

Reuter, M., Buchwitz, M., Schneising, O., Heymann, J., Bovensmann, H., and Burrows, J. P.: A method for improved SCIAMACHY CO_2 retrieval in the presence of optically thin clouds, Atmos. Meas. Tech., 3, 209–232, doi:10.5194/amt-3-209-2010, 2010.

Rothman, L. S., Jacquemart, D., Barbe, A., Chris Benner, D., Birk, M., Brown, L. R., Carleer, M. R., Chackerian Jr., C., Chance, K., Coudert, L. H., Dana, V., Devi, V. M., Flaud, J.-M., Gamache, R. R., Goldman, A., Hartmann, J.-M., Jucks, K. W., Maki, A. G., Mandin, J.-Y., Massie, S. T., Orphal, J., Perrin, A., Rinsland, C. P., Smith, M. A. H., Tennyson, J., Tolchenov, R. N., Toth, R. A., Vander Auwera, J., Varanasi, P., and Wagner, G.: The HITRAN 2004 molecular spectroscopic database, J. Quant. Spectrosc. Ra., 96, 139–204, 2005.

Sioris, C. E. and Evans, W. F. J.: Impact of rotational Raman scattering in the O_2 A band, Geophys. Res. Lett., 27, 4085–4088, 2000.

Sioris, C. E., Bazalgette Courreges-Lacoste, G., and Stoll, M.-P.: Filling in of Fraunhofer lines by plant fluorescence: Simulations for a nadir-viewing satellite-borne instrument, J. Geophys. Res., 108, 4133, doi:10.1029/2001JD001321, 2003.

Spurr, R. J. D., de Haan, J., van Oss, R., and Vasilkov, A. P.: Discrete ordinate radiative transfer in a stratified medium with first order rotational Raman scattering, J. Quant. Spectrosc. Ra., 109, 404–425, 2008.

Subhash, N. and Mohanan, C. N.: Curve-fit analysis of chlorophyll fluorescence spectra: Application to nutrient stress detection in sunflower, Remote Sens. Environ., 60, 347–356, 1997.

Yoshida, Y., Ota, Y., Eguchi, N., Kikuchi, N., Nobuta, K., Tran, H., Morino, I., and Yokota, T.: Retrieval algorithm for CO_2 and CH_4 column abundances from short-wavelength infrared spectral observations by the Greenhouse gases observing satellite, Atmos. Meas. Tech., 4, 717–734, doi:10.5194/amt-4-717-2011, 2011.

Zarko-Tejada, P. J., Miller, J. R., Mohammed, G. H., and Noland, T. L.: Chlorophyll fluorescence effects on vegetation apparent reflectance: I. Leaf-level measurements and model simulations, Remote Sens. Environ., 74, 582–595, 2000.